Bulk hadron production at high rapidities

G. I. Veres[a,b]

[a]Eötvös Loránd University, Department of Atomic Physics
Pázmány Péter sétány 1/A, H-1117, Budapest, Hungary

[b]Massachusetts Institute of Technology, Laboratory for Nuclear Science
77 Massachusetts Avenue, Bldg. 24-422, Cambridge, MA 02139, USA

Recent experimental observations on the 'bulk' features of particle production at high (pseudo)rapidities will be reviewed. This kinematic region is of interest mostly because of its relevance to the theoretical description of initial state effects of nuclei at ultra-relativistic energies. Measurements of the charged hadron multiplicity density as well as the pseudorapidity dependence of the elliptic and directed flow exhibit a remarkable scaling property as a function of collision energy. This scaling seems to hold for pions and even photons and J/Ψ-s, but is violated for protons. The special role of baryons will be discussed using selected results on nuclear transparency and baryon stopping.

1. INTRODUCTION

1.1. Motivation

The focus of research in relativistic heavy ion collisions initially has been toward the mid-rapidity region. This is justified in the context of the search for the new phase of QCD at high temperatures (energy density), the Quark Gluon Plasma, the emergence of which was expected at midrapidity. In addition, an extended Lorentz-invariant central plateau was predicted in the (charged) particle rapidity distribution [1]. Most experiments have been designed with good midrapidity-coverage in mind. At earlier fixed target experiments, particle detection closer to beam (target) rapidity was less difficult than at high energy colliders.

In heavy ion collisions, the existence of a boost-invariant *central* region is not confirmed experimentally. On the other hand, several observables in the *high rapidity* region are found to scale in a simple way as a function of energy. Furthermore, most of the baryons are emitted at high rapidity, and their energy loss is of primary interest, since it is related to the created energy density. The total number of produced charged particles per participant nucleon (N_{part}) pair does not depend on the centrality of the heavy ion collision. There is a remarkable balance of the centrality dependent midrapidity and high rapidity particle yields [2], suggesting a deeper connection between these two regions.

At RHIC, a suppression of high-p_T particles at high rapidities is observed in d+Au collisions [3], which is interpreted as the saturation of the gluon density of the ultra-relativistic Au nucleus at low Bjorken-x values [4]. Measurements at high rapidity are necessary to

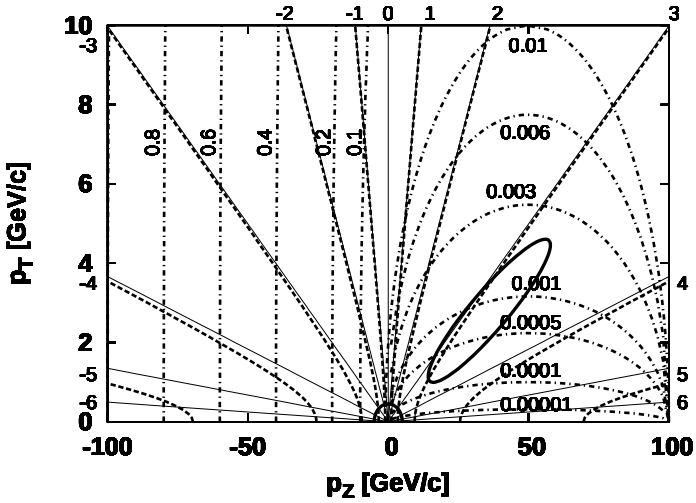

Figure 1. Constant y (dashed lines, for proton mass), η (thin solid lines) and $x_{\rm Bj}$ (dash-dotted lines) contours in the p_T vs. p_Z plane for the highest RHIC energy. (See the text for details.) The PHOBOS acceptance for very low p_T [14] (low-$x_{\rm Bj}$ and low $\rm Q^2$), and part of the BRAHMS acceptance at high η (low-$x_{\rm Bj}$ and higher $\rm Q^2$) are shown by ellipses.

reach small enough x values but still have a large enough momentum transfer ($\rm Q^2$) for this interpretation to apply. However, it is not easy to disentangle which physical processes (Cronin-effect, shadowing, energy loss, initial state gluon saturation, fragmentation of partons at high rapidities, etc.) influence the observed final hadron yields.

There is a large amount of data available on collisions of simpler systems (p+p, p+A) partially still under analysis. Baryon stopping and nuclear transparency is a large field of study in itself, and is also related to basic questions about the carriers of baryon number. Parton energy loss in the QGP and in cold nuclei are at the center of attention ever since the discovery of the suppression of high p_T particle yields ('jet quenching') [5]. The observed baryon 'anomaly' (unexpectedly high p/π^+ and $\overline{p}/\pi^-$ ratios at high p_T) [6] suggests another connection between dynamics of baryons at midrapidity in the transverse direction, and baryon transport in the longitudinal direction [7]. A non-exhaustive set of measurements will be discussed here, to illustrate some of the thoughts outlined above.

1.2. Kinematics of saturation physics

Various kinematic variables are used to study high rapidity phenomena and saturation physics, where the largest depletion of gluon density is expected at low $x_{\rm Bj}$ and high $\rm Q^2$; experiments have to focus on that region. Fig. 1 shows constant rapidity (y, dashed lines, for proton mass), and pseudorapidity (η, thin solid lines) lines of final state particles in the transverse (p_T) vs. longitudinal momentum (p_Z) plane for the highest RHIC energy (100 GeV/nucleon colliding beams). As an illustration, constant Bjorken-x ($x_{\rm Bj}$) lines of partons probed in the Au nucleus are also plotted (dash-dotted lines, ignoring mass) for a d+Au collision (with the Au nucleus moving from right to left)[1]. A fourth variable, Feynman-x (not shown) is defined as $x_F = 2p_Z/\sqrt{s_{\rm NN}}$, thus $x_F \approx x_{\rm Bj}$ for large $x_{\rm Bj}$.

[1]We use a great simplification here: we think of the d projectile as the incoming 'lepton' and the final state particle as the outgoing 'lepton', and borrow the definition of $x_{\rm Bj}$ from Deep Inelastic Scattering.

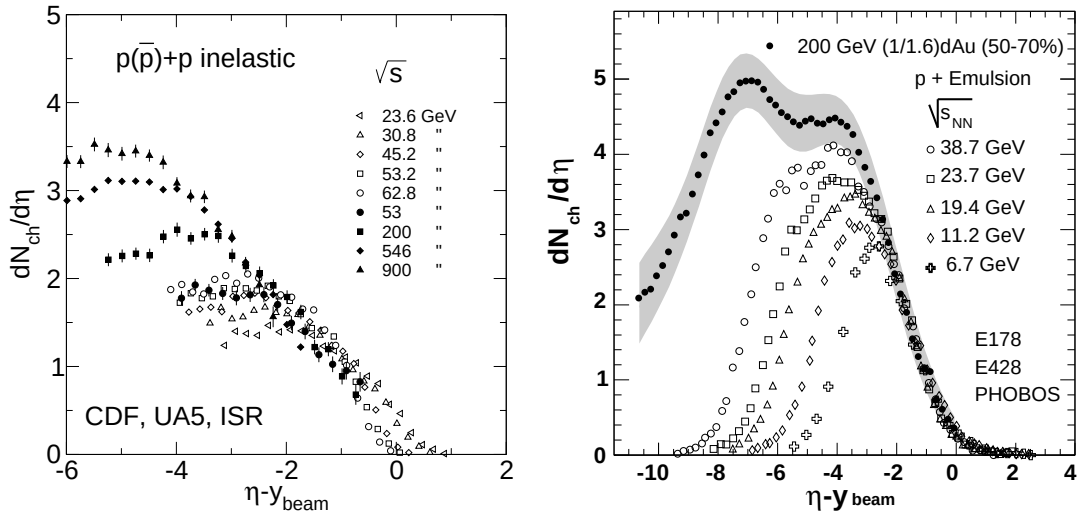

Figure 2. Pseudorapidity density distributions of charged particles emitted in $p(\overline{p})+p$ (left panel) and d+Au, p+Emulsion (right panel) collisions at various energies as a function of the $\eta' = \eta - y_{\rm beam}$ variable [17–20]. For details of the normalization of the data in the right panel see [19].

1.3. Experimental capabilities

At RHIC, several detectors cover the high rapidity region. The STAR experiment has the Photon Multiplicity Detector [8] ($2.3 < \eta < 3.8$), Forward TPC [9] ($2.5 < |\eta| < 4.0$), Forward π^0 Detector [10] ($3.3 < \eta < 4.1$) and the planned Forward Meson Spectrometer ($2.5 < \eta < 4.0$). The PHENIX experiment can use the muon stations to measure hadron yields at high rapidities ($1.4 < |\eta| < 2.2$), using the decay length dependence of the $K^{\pm} \rightarrow \mu^{\pm}\nu_{\mu}(\overline{\nu_{\mu}})$ and $\pi^{\pm} \rightarrow \mu^{\pm}\nu_{\mu}(\overline{\nu_{\mu}})$ decays, or observing punch-through hardons [11]. The BRAHMS spectrometers cover a large pseudorapidity region ($\eta < 3.5$) with particle-ID using Ring Imaging Čerenkov Detectors [12]. Finally, the largest η acceptance (although with no particle identification) is offered by the PHOBOS Multiplicity Array $|\eta| < 5.4$ [13]. As examples, the PHOBOS acceptance for very low p_T [14] (low-$x_{\rm Bj}$ and low Q^2), and the BRAHMS acceptance at high η (low-$x_{\rm Bj}$ and higher Q^2) are illustrated in Fig. 1. The low $x_{\rm Bj}$ and high Q^2 region is at high η and high p_T. At RHIC, this kinematic window is rather narrow, however, a large momentum space window to study low-$x_{\rm Bj}$ physics will be available, even at midrapidity, to the future LHC experiments. The CMS experiment plans to cover an extensive range of pseudorapidity ($|\eta| < 6.9$) with its calorimeters [15].

2. ENERGY DEPENDENCE OF PARTICLE PRODUCTION AT HIGH η

2.1. Inclusive charged particle spectra

One of the simple ways to study particle production at high rapidity is to compare charged particle η distributions measured at various collision energies. The η'=η-$y_{\rm beam}$ variable is used. It is measurable without particle identification and approximately transforms the distributions to the rest frame of one of the colliding particles/ions.

In proton-proton collisions, the so called *limiting fragmentation* [16] is seen from a few GeV to 900 GeV collision energy (e.g. at CDF, UA5 and ISR [17]). The left panel of Fig. 2 shows that the charged particle pseudorapidity density distributions are approximately

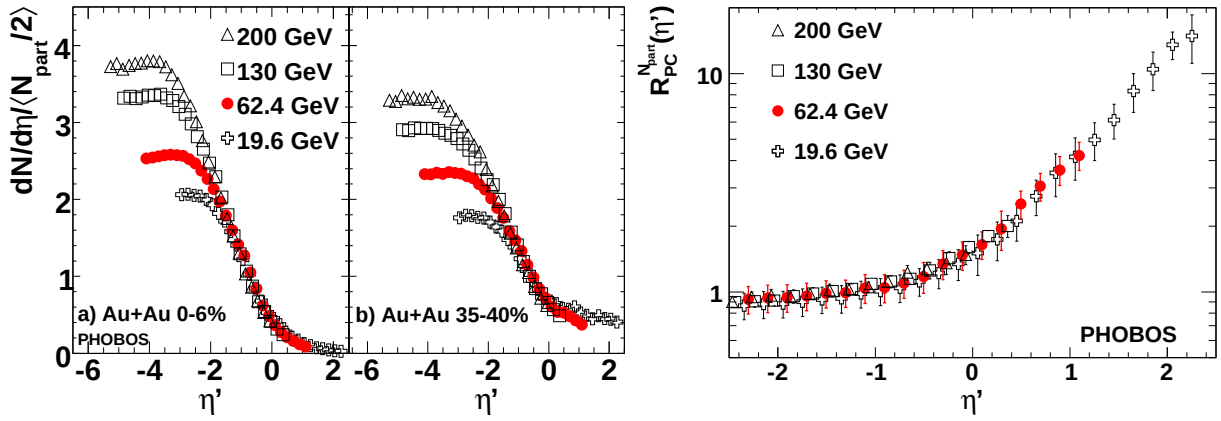

Figure 3. Left panel: distributions of pseudorapidity density of charged particles emitted in a) central, b) peripheral Au+Au collisions at various energies as a function of $\eta' = \eta - y_{\rm beam}$, normalized by the average number of participant nucleon pairs. Right panel: ratio of η' distributions in peripheral and central Au+Au collisions, normalized to the number of participant pairs [21].

independent of collision energy over a large range of η', which grows with $\sqrt{s}$.

As the right panel of Fig. 2 shows, similar scaling was observed for p+A collisions between $\sqrt{s_{\rm NN}} = 6.7$ and 38.7 GeV [18], and more recently in d+Au collisions at $\sqrt{s_{\rm NN}} =$ 200 GeV [19,20]. The observed energy-independence of these distributions holds both for the projectile and for the target reference frames, i.e. for $\eta \pm y_{\rm beam}$ [19].

In heavy ion collisions at RHIC energies, the BRAHMS and PHOBOS experiments have collected a large and systematic dataset on $dN/d\eta$ distributions, at $\sqrt{s_{\rm NN}}$= 19.6, 62.4, 130 and 200 GeV energies in Au+Au [2,22], and at 62.4 and 200 GeV energies in Cu+Cu collisions [21]. Instead of a sizeable plateau at midrapidity, similarly to p+p and p+A collisions, an extended longitudinal scaling region around $\eta' = 0$ is observed, as shown in the left panel of Fig. 3. One can visualize this scaling by imagining that the energies of the two colliding beams are adjustable separately. If one holds the energy of the first beam constant while increasing the energy of the second beam (in which the low-x gluons become more and more saturated), the particle density measured at a fixed η increases only up to a limit, given by the limiting curve in Fig. 3, where it saturates. This longitudinal scaling holds for Au+Au events with the same collision centrality (same number of participants), but the limiting curve is different for central and for peripheral events. The ratio of $dN/d\eta'$ distributions in peripheral to central Au+Au collisions is found to be energy independent to a remarkable precision over an order of magnitude in $\sqrt{s}$, as shown in the right panel of Fig. 3.

Longitudinal scaling is compatible with the Color Glass Condensate picture. The application of gluon saturation and standard parton fragmentation to the high rapidity region leads to such a limiting curve [23]. This prediction is shown in the left panel of Fig. 4, and is in good agreement with the data.

Of course, the theoretical description breaks down at a certain η' value, as the probed $x_{\rm Bj}$ in the projectile increases. The centrality dependence of the $dN/d\eta$ distributions is also correctly described by the Color Glass Condensate model [24].

The predictions of various model calculations for $dN/d\eta$ at $\eta = 0$ in central Pb+Pb

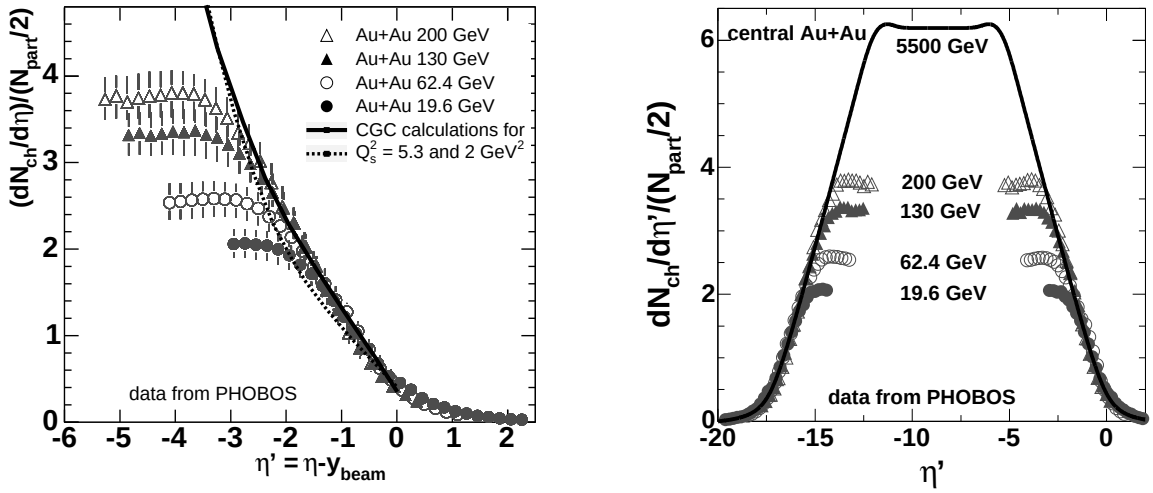

Figure 4. Left panel: $dN/d\eta'$ distributions of charged particles emitted in central Au+Au collisions at various energies as a function of $\eta' = \eta - y_{\rm beam}$, normalized by the average number of participant nucleon pairs, together with CGC calculations [23]. Right panel: extrapolation to LHC energy based on *linear* limiting curve and *logarithmic* rise of midrapidity density with $\sqrt{s}$ [26].

collisions at the LHC ($\sqrt{s_{\rm NN}}$=5500 GeV) range between 1000 and 7000. Based on the simple assumptions that the limiting curve of the $dN/d\eta'$ distributions is linear (as seems to be the case at RHIC energies) and that the observed logarithmic increase of $dN/d\eta|_{\eta=0}$ with $\sqrt{s_{\rm NN}}$ continues to be valid [25], one can estimate the central $dN/d\eta$ to be about 1100 and the total number of charged particles created to be about 14000 at the LHC [26], see the right panel of Fig. 4.

2.2. Identified particles

The scaling properties discussed so far are more surprising if one considers the different production mechanism of various particle species. The abundance of the lightest mesons indicate the amount of entropy created (in a thermodynamical picture). The amount of net baryons ($B - \overline{B}$) however is a conserved quantity, and the amount of stopping of the initial baryons in the colliding nuclei gives rise to the energy necessary for meson production as well as baryon pair production.

There are extensive measurements of the rapidity distributions of charged pions [27–29], protons and antiprotons [27,30,31] in heavy ion collisions. As shown in Fig. 5 for collision energies between 2.63 and 200 GeV per nucleon pair, the charged pion production, observing it in the rest frame of one of the projectiles, shows a similar scaling behaviour as the charged hadrons as a whole. The recent measurement of the neutral pion yield at high rapidities at 62.4 GeV [32] follows the scaling observed for the charged pions rather precisely. A similar scaling of net proton distributions is not expected because of baryon conservation and a widening of the rapidity gap with increasing energy. The right panel of Fig. 5 is a compilation of dN/dy distributions of protons (below $\sqrt{s_{\rm NN}}$=5 GeV) and net protons (at $\sqrt{s_{\rm NN}}$=17.27 and 200 GeV).

The natural question arising is whether this longitudinal scaling at high rapidity is a fundamental feature of particle production, or a remarkable coincidence, considering that

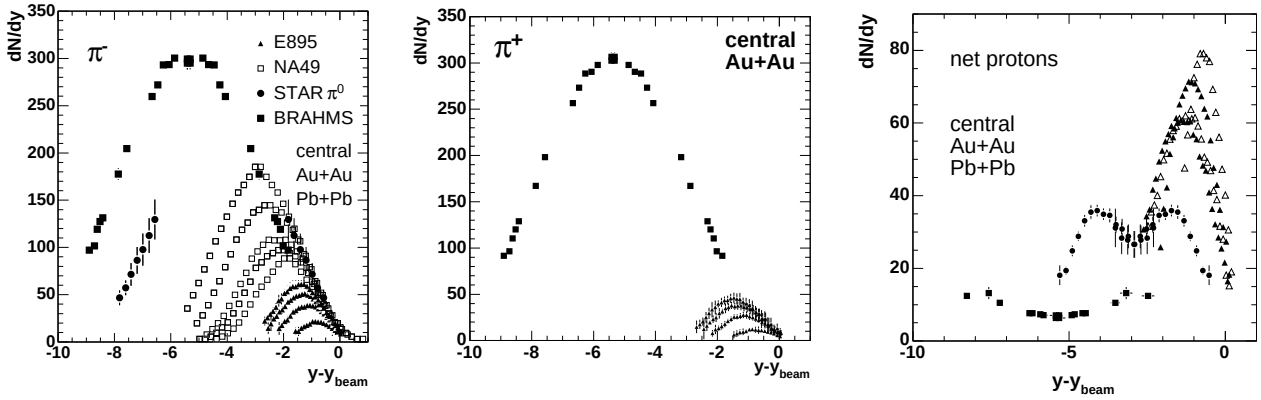

Figure 5. Rapidity (y'=y-$y_{\rm beam}$) distributions of π^- and π^+ particles and net protons ($p-\overline{p}$) produced in central Au+Au (Pb+Pb) collisions at $\sqrt{s_{\rm NN}}$ = 2.63, 3.28, 3.84, 4.29 [27], 6.27, 7.62, 8.76, 12.32, 17.27 [28,30] and 200 GeV [29,31], and π^0-s at 62.4 GeV [32].

many effects (baryon stopping, gluon saturation, collective effects, parton fragmentation etc.) play a role at the same time. Naturally, the scaling behaviour cannot hold equally precisely for all charged particles and for only mesons, since the dynamics of baryon stopping and production is fundamentally different. This could perhaps explain why the limiting curve for charged particles appears to be centrality dependent, as opposed to photons - originating mostly from π^0 decays [32]).

2.3. Feynman-x scaling of various final states

A frequently used way of quantifying longitudinal scaling and target size dependence of particle production in p+A collisions is to study the α exponent in the relation $\sigma_{\rm pA} = \sigma_0 A^\alpha$. This is done by measuring the $\sigma_{\rm pA}$ production cross sections as a function of the target nuclear mass, A, and as a function of the Feynman-x variable. The left panel of Fig. 6 is a compilation of data showing various final states and collision energy in p+A collisions [34]. This shows that the attenuation as a function of x_F is remarkably uniform within the experimental uncertainties. A more recent measurement of J/Ψ mesons in d+Au collisions at $\sqrt{s_{\rm NN}}$=200 GeV [33] is compared to lower energy data (right panel of Fig. 6) and also exhibits the x_F scaling with energy. However, the same scaling does not hold if the same data is plotted as a function of the $x_{\rm Bj}$ variable (referring to the Au nucleus). This indicates that the way in which gluon saturation plays a role in the J/Ψ production is strongly energy dependent (middle panel of Fig. 6).

In the following section more details about the centrality dependence of hadron production (and baryon stopping) at high rapidities are discussed.

3. BARYON STOPPING AND NUCLEAR TRANSPARENCY

It is apparent from the previous sections, that the dynamics of the energy loss by the initial baryons in a heavy ion collision strongly influences particle production (at high rapidities). Baryon energy loss in the hot medium created in heavy ion collisions (A+A) and in cold nuclear matter (p+A, d+A) has been studied and compared extensively (e.g. [34–37]). In addition, baryons are observed to behave differently than mesons when studying the 'jet quenching' of different species, leading to the baryon 'anomaly' at RHIC [6].

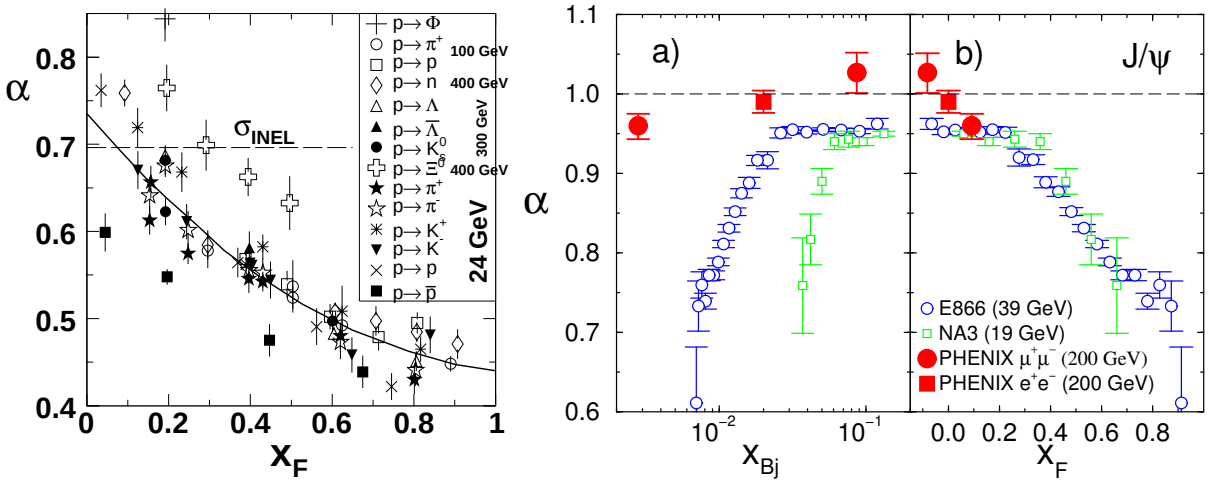

Figure 6. Scaling of the production of $\Phi, \pi^+, \pi^-, p, \overline{p}, n, \Lambda, \overline{\Lambda}, K^0_s, \Xi^0, K^+, K^-$ and J/Ψ particles as a function of x_F (left and right panels) and $x_{\rm Bj}$ in the target nucleus (middle panel) in p+A [34] and d+Au [33] collisions at $\sqrt{s_{\rm NN}}$=19, 39 and 200 GeV.

Among the earlier puzzles on nuclear transparency is the independence of the $\Lambda/\overline{\Lambda}$ ratio on the size of the target nucleus (left panel of Fig. 7) seen in minimum bias p+A collisions at 300 GeV beam energy on fixed target [38]. A complete attenuation in the cold nucleus, which would restrict particle production to the nuclear surface, may seem to be a plausible explanation. Preliminary data on Λ hyperons at RHIC [39] show that this ratio is independent of centrality in d+Au collisions (second panel in Fig. 7). However, the dN/dy yield of net lambdas ($\Lambda-\overline{\Lambda}$) strongly depends on target size and centrality, showing clear evidence of more baryon stopping for larger targets and central collisions, shown in the two rightmost panels of Fig. 7 (200 GeV proton beam on fixed Au and S targets [40] and d+Au collisions at $\sqrt{s_{\rm NN}}$=200 GeV [39]). Similar observations have been made for the $p/\overline{p}$ ratio and for the net protons ($p-\overline{p}$), see for example [40]. Interestingly, in d+Au and Au+Au collisions at $\sqrt{s_{\rm NN}}$=200 GeV energy, the $p/\overline{p}$ ratio does not, or only weakly depends on centrality at midrapidity [41], while the amount of net protons is a strong (in fact *linear*) function of the number of participants in Au+Au collisions at $\sqrt{s_{\rm NN}}$=62.4 and 200 GeV [42]. Other studies of p+Pb and Pb+Pb collisions at SPS have also shown that while there is no complete attenuation for baryons, the net proton distributions have a very strong centrality dependence. Remarkably, the stopping is stronger in central p+Pb than central Pb+Pb collisions, even if samples with the same average number of binary nucleon-nucleon collisions per participant are compared [35–37].

In *central* Au+Au collisions at $\sqrt{s_{\rm NN}}$=200 GeV, the average rapidity loss of the incoming baryons was estimated to be about two units [31], and a similar value was obtained earlier for *minimum bias* p+A collisions [43]. Furthermore, baryon stopping (the rapidity distribution of $p-\overline{p}$) was found not to depend on the size of the projectile nucleus as long as it was smaller than the target nucleus and the collision was central [40].

The examples above show that it is not only necessary to understand baryon stopping to separate it from other physically important phenomena. To reach the correct conclusions, one must consider the relation of high- and mid-rapidity physics, small and large colliding systems and the centrality dependence of the various observables, all at the same time.

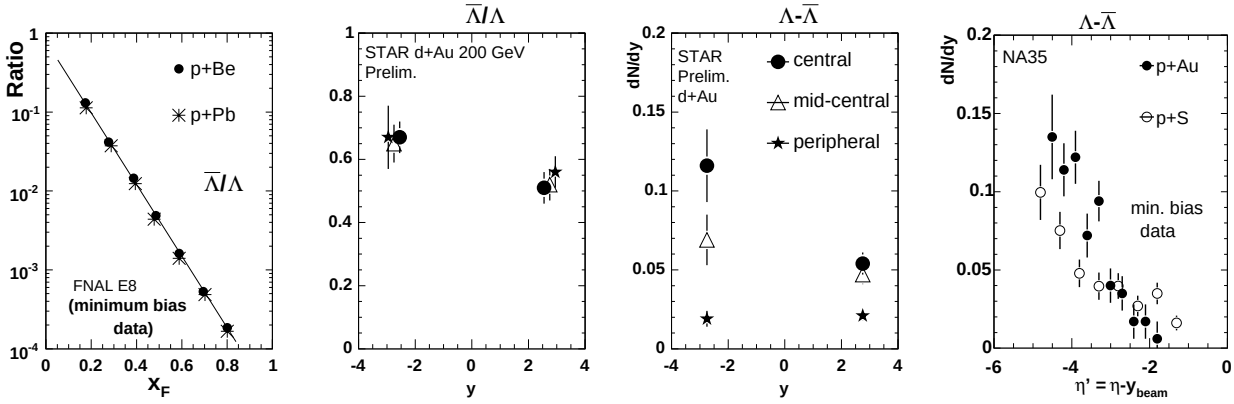

Figure 7. $\Lambda/\overline{\Lambda}$ ratio vs. x_F from [38] in p+A collisions (300 GeV protons on fixed target); the same ratio in d+Au collisions at $\sqrt{s_{\rm NN}}$=200 GeV from [39] (preliminary data); the net Λ rapidity distribution from [39]; and in min. bias p+A collisions at the SPS [40].

Studies of baryon stopping may also be able to address profound physical questions about the nature and carriers of baryon number. As an example, the HIJING B$\overline{\rm B}$ 2.0 model including *baryon junctions* can describe the rapidity dependence of *both* the $p/\overline{p}$ ratio *and* the net baryon density in 200 GeV Au+Au collisions [7].

4. AZIMUTHAL ASYMMETRY OF HIGH-η PARTICLE PRODUCTION

One of the important 'bulk features' of hadron production at high rapidities is the asymmetry of the azimuthal distribution of particles around the beam direction, relative to the reaction plane ('flow'). This asymmetry can be elliptical, characterized by the v_2 coefficient, as well as off-center or 'directed', characterized by the v_1 coefficient of its Fourier-expansion. This flow is a signature of collective, final state effects, as opposed to the gluon saturation at low $x_{\rm Bj}$, which is truly a feature of the *initial* state in the collision. Thus, the saturation picture alone cannot account for the large v_2 values observed in A+A collisions at RHIC. Furthermore, there is no reason to expect that similar longitudinal scaling would exist for the flow observables, as it did for the $dN/d\eta'$ distributions in that picture. In fact scaling is found to hold [21,44], as can be seen in Fig. 8, both for the v_2 and the v_1 variables, in Au+Au collisions from 19.6 to 200 GeV[2]. The elliptic flow data are well described by an analytical hydrodynamic model assuming ideal fluid dynamics [46]. This agreement illustrates how important *final* state interactions are for particle distributions at high rapidities.

5. SUMMARY

In summary, an extensive amount of data on hadron production at high rapidities has been collected and is currently under analysis and interpretation. From these data only a few results could be selected for discussion. Longitudinal scaling of $dN/d\eta$ and dN/dy distributions has been observed as a function of energy for pions and charged hadrons but not for protons. Scaling features, the centrality dependence and $dN/d\eta$ distributions are

[2]Note that the strong η dependence of v_2 was not observed by the BRAHMS experiment [45].

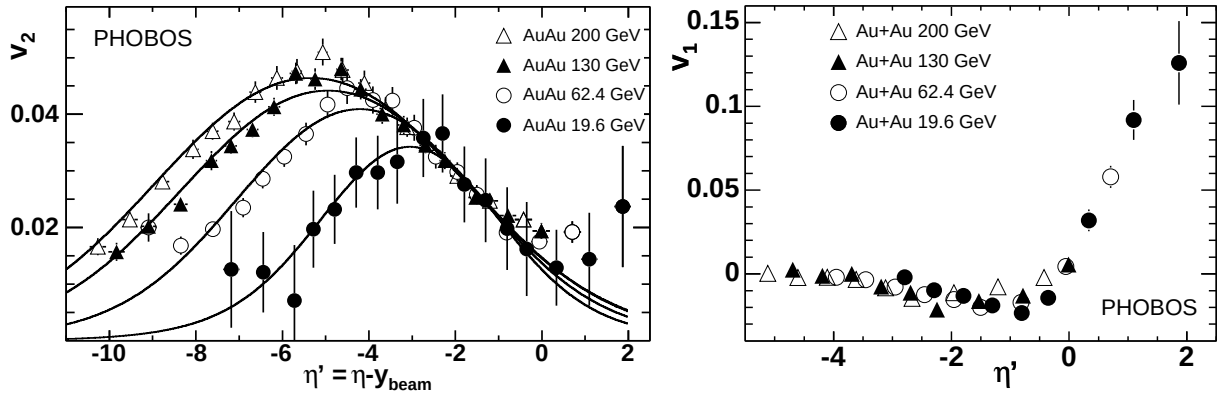

Figure 8. The v_2 measure of elliptic collective flow (left panel) and the v_1 measure of directed flow (right panel) in Au+Au collisions at $\sqrt{s}$ = 19.6, 62, 130 and 200 GeV energy, as a function of $\eta' = \eta - y_{\rm beam}$ [44,21]. (The centrality is 0-40% of the total inelastic cross section.) Theoretical curves were made using the Buda-Lund model [46].

successfully described by initial state gluon saturation models. However, baryon stopping (the influence of the valence structure of the projectile) also contributes to the final state hadron yields at high rapidity, following complicated dynamics having energy, centrality and target size dependence. Remarkably, another important 'bulk feature' of particle production, the azimuthal asymmetry, which is not explainable by initial state effects alone, still shows the same kind of longitudinal scaling (energy independence) in heavy ion collisions. Theoretical progress in describing high η (low-x) particle production in p+A and A+A collisions is rapidly progressing and generating a lot of interest. Nevertheless for a clean experimental isolation of initial state modifications of the incoming projectile one might have to turn to more differential measurements. Ideas to separate the various physical phenomena at high rapidities along with the new experiments at the LHC, will guide our theoretical understanding.

6. ACKNOWLEDGEMENTS

I am indebted to W. Busza, D. Röhrich, M. Gyulassy, R. Venugopalan, K. Itakura, G. Roland, T. Csörgő, M. Csanád, W. A. Zajc, B. Mohanty, C. Höhne, C. Blume, V. Topor-Pop, C. Loizides, R. Hollis, C. Henderson and F. Simon for the helpful discussions, and for providing me with their data. This work and participation at the Conference was possible due to the generous support from both of my Universities, from the Hungarian Scientific Research Fund under contracts T048898 and F049823, and from the János Bolyai Research Grant.

REFERENCES

1. J. D. Bjorken, Phys. Rev. D 27 (1983) 140.
2. B. B. Back *et al.* (PHOBOS Collaboration), Nucl. Phys. A 757 (2005) 28.
3. I. Arsene *et al.* (BRAHMS Collaboration), Phys. Rev. Lett. 93 (2004) 242303.
4. M. Gyulassy and L. McLerran, Nucl. Phys. A 750 (2005) 30.
5. K. Adcox *et al.* (PHENIX Collaboration), Phys. Rev. Lett. 88 (2002) 022301.

6. K. Adcox *et al.* (PHENIX Collaboration), Phys. Rev. C 69 (2004) 024904.
7. V. Topor-Pop *et al.*, Phys. Rev. C 70 (2004) 064906.
8. M. M. Aggarwal *et al.* (STAR Collaboration), Nucl. Instr. Meth. A499 (2003) 751.
9. K. H. Ackermann *et al.* (STAR Collaboration), Nucl. Instr. Meth. A499 (2003) 713.
10. J. Adams *et al.* (STAR Collaboration), Phys. Rev. Lett. 92 (2004) 171801.
11. S. S. Adler *et al.* (PHENIX Collaboration), Phys. Rev. Lett. 94 (2005) 082302.
12. M. Adamczyk *et al.* (BRAHMS Collaboration), Nucl. Instr. Meth. A 499 (2003) 437.
13. B. B. Back *et al.* (PHOBOS Collaboration), Nucl. Inst. Meth. A 499 (2003) 603.
14. A. Trzupek (for the PHOBOS Collaboration), these Proceedings.
15. M. Murray (for the CMS Collaboration), these Proceedings.
16. J. Benecke *et al.*, Phys. Rev. 188 (1969) 2159.
17. F. Abe *et al.* (CDF Collaboration), Phys. Rev. D 41 (1990) 2330.
    R. E. Ansorge *et al.* (UA5 Collaboration), Z. Phys. C 43 (1989) 75.
    W. Thome *et al.* (ISR), Nucl. Phys. B 129 (1977) 365.
18. J. E. Elias *et al.* (E178 Experiment), Phys. Rev. D 22 (1980) 13.
    I. Otterlund *et al.*, Nucl. Phys. B 142 (1978) 445. and references therein
    S. Fredriksson *et al.* Phys. Rept. 144 (1987) 187. and references therein
19. B. B. Back *et al.* (PHOBOS Collaboration), *arXiv:nucl-ex/0409021* (2004).
20. I. Arsene *et al.* (BRAHMS Collaboration), Phys. Rev. Lett. 94 (2005) 032301.
21. G. Roland (for the PHOBOS Collaboration), these Proceedings.
22. I. G. Bearden *et al.* (BRAHMS Collaboration), Phys. Rev. Lett. 88 (2002) 202301.
23. J. Jalilian-Marian, Phys. Rev. C 70 (2004) 027902.
24. J. Jalilian-Marian, J. Phys. G 30 (2004) S751.
25. B. B. Back *et al.* (PHOBOS Collaboration), Phys. Rev. Lett. 88 (2002) 22302.
26. W. Busza, Acta Phys. Polon. B 35 (2004) 2873.
27. J. L. Klay *et al.* (E895 Collaboration), Phys. Rev. C 68 (2003) 054905.
28. S. V. Afanasiev *et al.* (NA49 Collaboration), Phys. Rev. C 66 (2002) 054902.
29. I. G. Bearden *et al.* (BRAHMS Collaboration), Phys. Rev. Lett. 94 (2005) 162301.
30. H. Appelshauser *et al.* (NA49 Collaboration), Phys. Rev. Lett. 82 (1999) 2471.
31. I. G. Bearden *et al.* (BRAHMS Collaboration), Phys. Rev. Lett. 93 (2004) 102301.
32. J. Adams *et al.* (STAR Collaboration), Phys. Rev. Lett. 95 (2005) 062301.
33. S. S. Adler *et al.* (PHENIX Collaboration), *arXiv:nucl-ex/0507032* (2005).
34. W. Busza, Nucl. Phys. A 544 (1992) 49c.
35. G. I. Veres, poster at the Quark Matter 2001 Conference
36. Gábor I. Veres, *Ph.D. Thesis*, ELTE, Budapest (2001).
37. Andrzej Rybicki, *Ph.D. Thesis*, IFJ, Kraków (2002).
38. P. Skubic *et. al*, Phys. Rev. D 18 (1978) 3115.
39. F. Simon (for the STAR Collaboration), J. Phys. G 31 (2005) S1065.
40. T. Alber *et al.* (NA35 Collaboration), Eur. Phys. J. C 2 (1998) 643.
41. B. B. Back *et al.* (PHOBOS Collaboration), Phys. Rev. C 70 (2004) 011901(R).
42. Conor Henderson, *Ph.D. thesis*, Mass. Inst. Tech., Cambridge (2005) Fig. 6-8.
43. W. Busza and R. Ledoux, Ann. Rev. Nucl. Part. Sci. 38 (1988) 119.
44. B. B. Back *et al.* (PHOBOS Collaboration), Phys. Rev. Lett. 94 (2005) 122303.
45. H. Ito (for the BRAHMS Collaboration), these Proceedings.
46. M. Csanád, T. Csörgő, B. Lörstad and A. Ster, *arXiv:nucl-th/0510027* and *0509106*.